JAAS

CrossMark
click for updates

Bulk sensitive determination of the Fe^{3+}/Fe_{Tot}-ratio in minerals by Fe $L_{2/3}$-edge X-ray Raman scattering

Alexander Nyrow,†*[a] Christian Sternemann,*[a] John S. Tse,[b] Christopher Weis,[a] Christoph J. Sahle,‡[a] Kolja Mende,[a] D. C. Florian Wieland,§[a] Valerio Cerantola,‡[c] Robert A. Gordon,¶[d] Georg Spiekermann,[eg] Tom Regier,[f] Max Wilke[g] and Metin Tolan[a]

We present the first measurements of the iron $L_{2/3}$-edge of the compounds FeO, Fe_2O_3, and Fe_3O_4 at ambient pressure and of $FeCO_3$ at high pressures of 2.4 and 40 GPa using a diamond anvil cell by X-ray Raman scattering spectroscopy, a bulk sensitive probe of soft X-ray absorption edges making use of hard X-rays. We show that the spectral shape of the Fe $L_{2/3}$-edge can be analyzed quantitatively to reveal the oxidation state of iron in matter. Consequently, *in situ* X-ray Raman scattering spectroscopy at the iron L-edge at high pressure and temperature opens exciting perspectives to characterize the local coordination, oxidation, and spin state of iron at high pressure and temperature, conditions that are of relevance for *e.g.* geological sciences or chemical processing.

1 Introduction

Iron is one of the most common elements of the inner Earth, strongly affecting the macroscopic properties of related minerals, melts, and glasses.[1,2] Under pressure–temperature conditions of the deep Earth, the local chemical and physical properties of iron, *e.g.* oxidation state, local coordination, and spin state, can vary significantly.[3–5] Quantitative information about these parameters is used in order to understand the structural changes during geochemical and geophysical processes such as Fe–Mg partitioning, iron melting and density variations for instance associated with the spin crossover in iron. *In situ* experiments under the relevant thermodynamic conditions provide unique insights into geochemical and geophysical processes.[6,7]

[a]Fakultät Physik/DELTA, Technische Universität Dortmund, 44227 Dortmund, Germany. E-mail: alexander.nyrow@tu-dortmund.de; christian.sternemann@tu-dortmund.de

[b]Department of Physics and Engineering Physics, University of Saskatchewan, Saskatoon S7N 5E2, Canada

[c]Bayerisches Geoinstitut, Universität Bayreuth, D-95440 Bayreuth, Germany

[d]PNCSRF, APS Sector 20, Argonne, IL 60439, USA

[e]Deutsches Elektronen-Synchrotron DESY, D-22607, Hamburg, Germany

[f]CLS, 44 Innovation Boulevard, Saskatoon S7N 2V3, Canada

[g]Section 3.3, Deutsches GeoForschungsZentrum, 14473 Potsdam, Germany

† Present address: Max-Planck-Institute for Chemical Energy Conversion, D-45470 Mülheim.

‡ Present address: European Synchrotron Radiation Facility, F-38043 Grenoble Cedex, France.

§ Present address: Helmholtz-Zentrum Geesthacht, Institut für Werkstoffforschung, D-21502 Geesthacht, Germany.

¶ Present address: Moyie Institute, Port Coquitlam, BC, Canada.

Next to Mössbauer spectroscopy,[8,9] the local chemical environment of iron in minerals is often studied by X-ray absorption spectroscopy (XAS) at the Fe K-edge, which is a very sensitive tool to study the oxidation state and local coordination.[10–13] The related pre-edge features, which contain information on the Fe 3d states, are difficult to resolve and a high-resolution monochromator setup is needed. So far, XAS studies of the near edge structure *in situ* at high pressure are rare, and analysis of the main edge is used.[14] Moreover, the 3d state can be probed directly by resonant X-ray emission.[15] Information on the orbital and spin magnetic moment is obtained using X-ray magnetic circular dichroism[16] and X-ray linear magnetic dichroism.[17]

Fe $L_{2/3}$-edge spectroscopy (2p → 3d) is also a sensitive method in order to study the local properties of iron and is performed either using soft X-rays[18–20] or by electron-energy loss spectroscopy (EELS)[21–23] with a transmission electron microscope. Compared to pre-edge studies of the redox state at the Fe K-edge, the variation of the corresponding intensity parameter determined on the Fe L-edge is large, thus offering a potentially higher precision for determining the oxidation state. In other words, if there would be no experimental constraints for measuring either one of the edges, the L-edge should provide results with better precision. Therefore, measurements of the L-edge, if feasible, may be a valuable alternative where changes in the pre-edge of the K-edge are too small to be resolved. XAS and EELS at the L-edges at X-ray energies below 1 keV are used for applications in *e.g.* geology,[3,21,24] physics,[19,25–29] biology,[30,31] catalysis,[32–35] and materials science.[18,36] However, these techniques cannot be applied for *in situ* high pressure experiments owing to the highly absorbing sample environment, *e.g.* resistively or laser heated diamond anvil cells.

The potential of X-ray Raman scattering spectroscopy can be exploited for bulk sensitive *in situ* studies of low-energy X-ray absorption edges even for embedded samples.[37–43] Recently, *in situ* high pressure measurements of the Fe $M_{2/3}$-edge demonstrated the ability to track the pressure induced spin cross-over in FeS and to extract quantitative information about the crystal field splitting of the 3d states in iron.[44] The Fe $M_{2/3}$-edge is significantly modified by weak changes of the oxidation and spin state, but it is less sensitive to the local coordination.[45] Recently, magnetic circular dichroism of X-ray Raman scattering was observed at the iron $L_{2/3}$-edge of pure iron.[46] In general, measurements of the Fe $L_{2/3}$-edge by X-ray Raman scattering spectroscopy are a very good alternative for studies of the oxidation state, the local coordination, and the spin state of iron in compounds under geologically relevant conditions. In this paper we focus on the capability of X-ray Raman scattering spectroscopy to analyze the oxidation state of a sample both at ambient and at high pressure.

2 X-ray Raman scattering

X-ray Raman scattering (XRS), a non-resonant inelastic X-ray scattering technique, provides spectroscopic information on soft X-ray absorption edges similar to XAS and EELS but using high-energy X-rays.[47–51] Consequently, the local atomic and electronic structure can be probed bulk sensitively yielding information about *e.g.* oxidation state, spin state and local coordination. By scanning the energy loss in the vicinity of an electron binding energy, core level excitations can be studied both in the dipole and non-dipole limits.[48] The intensity of the scattered radiation is proportional to the dynamic structure factor, which is given for transition metals and rare-earth elements due to the strong interaction between the 3d electron and the hole wave functions by

$$S(q,\omega) = \sum_{f}\sum_{k=0}^{\infty} D_k |\langle f(r)|j_k(qr)|c(r)\rangle|^2 \times \delta(E_c - E_f + \hbar\omega) \quad (1)$$

with the sum over all final states f. The transition matrix elements are given by the initial state radial wave function $c(r)$ with the energy E_c, the final state wave function $f(r)$ with the energy E_f, and the k-th order Bessel function $j_k(qr)$ scaled by the corresponding transition probability D_k.[52] The dynamic structure factor in eqn (1) is presented in the limit of polycrystalline and powder samples, for which the angular dependence of the matrix element is averaged. With respect to the symmetry properties of the initial and final state wave functions only transitions with $k = 1$ (dipole) and $k = 3$ (octupole) are allowed for the particular p to d transition of the Fe $L_{2/3}$-edge.[52,53] The weight of each transition channel is governed by the magnitude $\hbar q$ of the momentum transfer vector, that can be tuned in an experiment by changing the scattering angle.

3 Experimental details

The XRS experiment was performed at beamline PNC/XSD 20-ID of the Advanced Photon Source employing the LERIX

spectrometer.[54] Here, 19 Si(444) analyzer crystals are arranged in a semicircle (radius of 1 m) covering an angular range from 9° to 171°, which results in a momentum transfer range from 0.7 $Å^{-1}$ to 8.7 $Å^{-1}$. The energy of the incident X-rays with an overall resolution of 1.0 eV was tuned by using a Si(111) monochromator. In order to measure the Fe $L_{2/3}$-edge, the energy of incident X-rays was scanned from 8.582 keV to 8.682 keV resulting in an energy loss interval from 670 eV to 770 eV, respectively. Polycrystalline FeO ($^{[6]}Fe^{2+}$, space group $Fm3m$, corresponding to the geologically relevant mineral wustite), Fe_2O_3 ($^{[6]}Fe^{3+}$, space group $R\bar{3}c$, corresponding to hematite), and Fe_3O_4 (corresponding to magnetite with a composition of 1/3 $^{[6]}Fe^{2+}$, 1/3 $^{[6]}Fe^{3+}$, and 1/3 $^{[4]}Fe^{3+}$) powders with a trace metal basis of 99.9%, 99.995%, and 99.99%, respectively, were measured without further treatment. The samples were characterized by X-ray diffraction at beamline BL9 of the DELTA synchrotron source.[55] Phase purity was found for Fe_2O_3 and Fe_3O_4 whereas FeO contained a small amount (<3%) of iron. The spectra were collected in 1.5 hours (FeO) and 4 hours (Fe_2O_3 and Fe_3O_4). Due to the small momentum transfer dependence of the shape of the Fe $L_{2/3}$-edge, the spectra were summed up over the entire q-range. Subsequently, a background described by a polynomial function was fitted to the energy loss values below 700 eV and subtracted from the data. This background subtraction procedure is similar to that typically applied to EELS data.[21] Finally, background corrected spectra were normalized to the integrated intensity in the energy loss region from 700 eV to 728 eV. For a general description of the XRS data analysis see ref. 56 and 57.

4 Results and discussion

The results of the XRS measurements of the Fe $L_{2/3}$-edges on FeO, Fe_2O_3, and Fe_3O_4 are presented in Fig. 1. The spin–orbit splitting for FeO given by the distance between the inflection points of the Fe L_3- and Fe L_2-edges can be estimated to be 12.8 ± 0.2 eV, which is in very good agreement with earlier results.[58] Significant spectral differences can be observed, if the Fe $L_{2/3}$-edge of FeO is compared to that of Fe_2O_3. The energy shift between the inflection points of the Fe L_3- (707.1 eV) and Fe L_2-edges (720.3 eV) of Fe_2O_3 results in a spin–orbit coupling of 13.2 ± 0.2 eV, which agrees very well with values obtained by EELS.[21,58] The shape of the Fe $L_{2/3}$-edge of Fe_3O_4 shows a very broad, asymmetric, and featureless maximum due to the contribution of both FeO- and Fe_2O_3-like Fe $L_{2/3}$-edge spectra.

A comparison of the XRS results with XAS and EELS data, *e.g.* published in ref. 19, 20 and 59, shows a very good agreement concerning the relative energy position and shape of the Fe $L_{2/3}$-edges, which is a surprising result considering the origin of the excitation mechanism of the experimental techniques. While only dipole transitions are probed by XAS, a certain momentum transfer contribution can be found in EELS. However, typical EELS measurements are performed at low scattering angles, which restrict electronic excitations to dipole-like transitions. In contrast, XRS spectra are in general strongly dominated by higher order transitions at high scattering angles. Although the momentum transfer dependence of the multiplet spectra is very
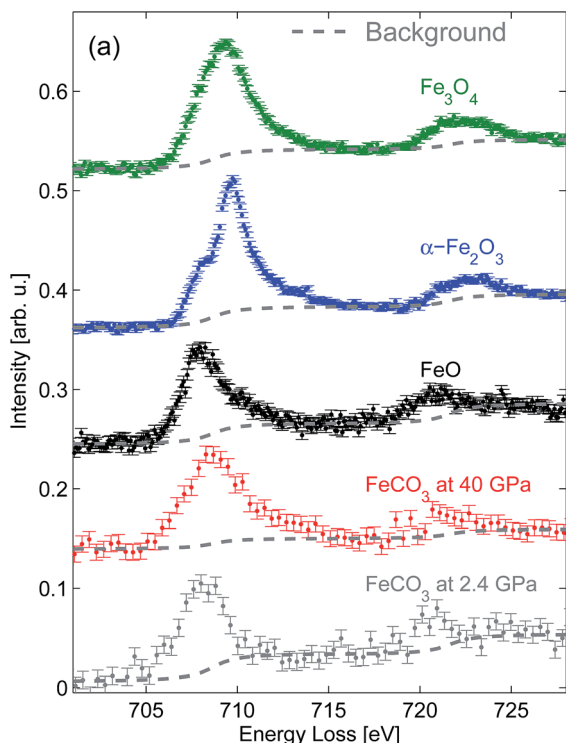
816 | *J. Anal. At. Spectrom.*, 2016, **31**, 815–820

This journal is © The Royal Society of Chemistry 2016

Fig. 1 Results of the Fe $L_{2/3}$-edge measurements of FeO (black), α-Fe_2O_3 (blue), and Fe_3O_4 (green) at ambient pressure. Moreover, the spectrum of $FeCO_3$ measured *in situ* at 2.4 GPa (grey) and 40 GPa (red) using a diamond anvil cell is presented. The gray dashed line represents a background modeled by a double arc-tangent function. The spectra are vertically shifted for a better overview.

strong for transition metals,[45,52,60] it is hardly observed at the Fe $L_{2/3}$-edge of FeO, Fe_2O_3 and Fe_3O_4. The ability to access non-dipole excitations is governed by the absolute value of the momentum transfer as well as the length scale of the effective radial overlap between the initial and final state wave functions, which is small for the 2p and 3d wave functions of iron. Thus, the momentum transfer range examined in this study is too small to get significant higher order contributions and the statistical accuracy of the spectra can be significantly enhanced due to the fact that the signal collected at different scattering angles by using multi-element spectrometers can be summed up.

The collected spectra can be employed to extract quantitative information about the Fe^{3+}/Fe_{Tot}-ratio. Therefore, the position and spectral shape of the Fe $L_{2/3}$-edge can be used as an indicator of the oxidation state and several extraction algorithms are discussed in the literature (see *e.g.* ref. 23). In order to obtain the Fe^{3+}/Fe_{Tot}-ratio, Garvie and Buseck[61] propose to fit Fe^{2+} and Fe^{3+} references to a spectrum taken on a mixed oxidation state sample. This algorithm is only applicable for materials with identical end-members and coordination of iron, which is not the case for Fe_3O_4. Alternatively, a series of analytical functions, *e.g.* Gaussian- or Lorentzian-type, can be fitted instead of reference spectra. The position and relative intensities of the series of analytical functions contain information about the

Fe^{3+}/Fe_{Tot}-ratio and local coordination of iron. However, several profiles with a large number of free parameters must be used in order to obtain accurate results.[22,62] Another alternative proposed by van Aken *et al.*[21] exploits the intensity ratio between the Fe L_3-edge and the Fe L_2-edge, which strongly depends on the Fe^{3+}/Fe_{Tot}-ratio contained in the material. The applicability of this algorithm was demonstrated for different examples of high-spin iron species with a variable oxidation state. Keeping in mind that this procedure can only be applied for high-spin iron species with conserved site symmetry,[20] the algorithm will be discussed in detail and applied to the XRS data in order to demonstrate the potential of XRS measurements to obtain quantitative information about the Fe^{3+}/Fe_{Tot}-ratio in the following.

The Fe $L_{2/3}$-edge measurements presented in Fig. 1 are further analyzed in order to remove the contribution of the excitations into the continuum states by subtracting a double arc-tangent function with the fixed inflexion points at 708.65 eV and 721.65 eV, respectively.[21] The resulting arc-tangent background for FeO, Fe_2O_3, and Fe_3O_4 is shown in Fig. 1. Subsequently, background corrected spectra shown in Fig. 2 are integrated in the energy loss ranges from 708.5 eV to 710.5 eV ($I(L_3)$) and from 719.5 eV to 721.5 eV ($I(L_2)$), as suggested by van Aken *et al.*[21] The intensity ratio $I(L_3)/I(L_2)$ is then correlated with the Fe^{3+}/Fe_{Tot}-ratio x of well characterized samples *via*

$$\frac{I(L_3)}{I(L_2)} = \frac{1}{ax^2 + bx + c} - 1 \qquad (2)$$

with $a = 0.183 \pm 0.011$, $b = -0.455 \pm 0.015$ and $c = 0.368 \pm 0.005$. Eqn (2) can be used as a calibration curve to determine the Fe^{3+}/Fe_{Tot}-ratio in unknown minerals by calculating their relative intensity $I(L_3)/I(L_2)$. van Aken *et al.* suggest that EELS would provide access to the Fe oxidation state on the particle length scale of 10 to 100 nm with a precision of 0.03 to 0.04 in terms of Fe^{3+}/Fe_{Tot}, which is similar to Mössbauer spectroscopy. In order to prove the applicability of this algorithm to the XRS results, $I(L_3)/I(L_2)$ was calculated for FeO ($Fe^{3+}/Fe_{Tot} = 0$), Fe_2O_3
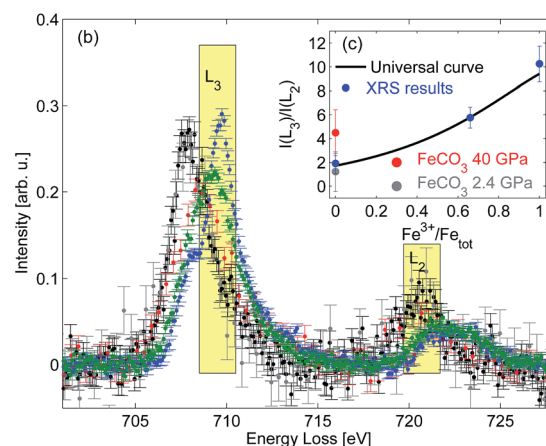

Fig. 2 Background corrected XRS spectra with indicated integration ranges; inset: calculated $I(L_3)/I(L_2)$ fractions as a function of the Fe^{3+}/Fe_{Tot} ratio in comparison with the calibration curve proposed by van Aken *et al.*[21]

($Fe^{3+}/Fe_{Tot} = 1$) and Fe_3O_4 ($Fe^{3+}/Fe_{Tot} = 0.67$). A comparison between evaluated intensity ratios on the basis of XRS measurements with the calibration curve determined by van Aken *et al.* is shown in the inset of Fig. 2. Our data indicate that this technique may be transferred to XRS and thus has the potential of gaining precise redox information using a bulk sensitive probe for samples with a larger grain size where XAS and EELS are not appropriate. Particularly, for *in situ* high pressure experiments the XRS technique may provide new ways of studying Fe redox equilibria.

In order to demonstrate the potential of this method to determine the iron oxidation state *in situ* under extreme conditions we performed a high pressure XRS measurement at beamline ID20 of ESRF (European Synchrotron Radiation Facility) using a multiple analyzer spectrometer.[57] An $FeCO_3$ single crystal ($^{[6]}Fe^{2+}$, space group $R\bar{3}c$ corresponding to siderite) was loaded in a Böhler–Almax diamond anvil cell using a rhenium gasket and helium as the pressure medium to guarantee quasi-hydrostatic conditions at high pressure. The sample with dimensions of about 15 μm × 25 μm × 25 μm was measured for 12 hours at 2.4 GPa and 8 hours at 40 GPa. The pressure was determined *via* the ruby fluorescence method.[63] The analyzer energy was 12.92 keV and the incident energy was scanned from 13.623 keV to 13.663 keV with an overall energy resolution of 2.1 eV at a momentum transfer of 3.2 ± 0.9 Å^{-1}. The spectra were analyzed as discussed above. The results obtained at 2.4 GPa are presented in Fig. 1 and show a good agreement with the FeO spectral shape despite the different energy resolution. Following the analysis procedure of van Aken *et al.*[21] (see Fig. 2) the extracted Fe^{3+}/Fe_{Tot} ratio fits to the universal curve within the accuracy of the experiment. The deviation between the L-edge's shape measured at 40 GPa and thus the change of the $I(L_3)/I(L_2)$ ratio compared to 2.4 GPa is due to the fact that the high spin to low spin transition already started.[64] This clearly confirms that the analysis by van Aken is strictly limited to iron compounds in the high spin state. The different energy resolution achieved with XRS and EELS does not affect the results of this analytical procedure. However, both the energy resolution and statistical accuracy can be improved in future experiments, which clearly demonstrates the feasibility of *in situ* measurements of the Fe L$_{2/3}$ edge at high pressure to evaluate the redox state.

5   Conclusion

In this paper, bulk sensitive measurements of the Fe L$_{2/3}$-edge by XRS spectroscopy are presented and their sensitivity to the oxidation state of iron is discussed for the examples of FeO, Fe_2O_3, and Fe_3O_4. Relative intensities of the spectral features of the Fe L$_{2/3}$-edge are used to extract quantitative information about the Fe^{3+}/Fe_{Tot}-ratio using the calibration curve by van Aken *et al.*[21] This approach is a prospective method to study the oxidation and spin state of iron bulk sensitively *in situ* under high pressure and high temperature conditions beyond the limits of other experimental techniques. The feasibility of *in situ* measurements under high pressure conditions using a diamond anvil cell was successfully demonstrated with the example of $FeCO_3$ probed at 2.4 GPa and 40 GPa.

References

1 J. Badro, G. Fiquet, F. Guyot, J.-P. Rueff, V. V. Struzhkin, G. Vankó and G. Monaco, *Science*, 2003, **300**, 789–791.
2 T. S. Duffy, *Nature*, 2008, **451**, 269–270.
3 C. McCammon, D. Frost, J. Smyth, H. Laustsen, T. Kawamoto, N. Ross and P. van Aken, *Phys. Earth Planet. Inter.*, 2004, **143144**, 157–169.
4 M. Wilke and H. Behrens, *Contrib. Mineral. Petrol.*, 1999, **137**, 102–114.
5 A. Zerr and R. Boehler, *Nature*, 1994, **371**, 506–508.
6 I. J. Parkinson and R. J. Arculus, *Chem. Geol.*, 1999, **160**, 409–423.
7 B. J. Wood and D. Virgo, *Geochim. Cosmochim. Acta*, 1989, **53**, 1277–1291.
8 *Mössbauer Spectroscopy*, ed. D. P. E. Dickson and F. J. Berry, Cambridge University Press, 1986.
9 T. Glaser, *Angew. Chem., Int. Ed.*, 2011, **50**, 10019–10020.
10 A. J. Berry, G. M. Yaxley, A. B. Woodland and G. J. Foran, *Chem. Geol.*, 2010, **278**, 31–37.
11 M. Munõz, V. de Andrade, O. Vidal, E. Lewin, S. Pascarelli and J. Susini, *Geochem., Geophys., Geosyst.*, 2006, **7**, Q11020.
12 M. Wilke, C. Schmidt, F. Farges, V. Malavergne, L. Gautron, A. Simionovici, M. Hahn and P.-E. Petit, *Chem. Geol.*, 2006, **229**, 144–161.
13 M. Wilke, O. Hahn, A. B. Woodland and K. Rickers, *J. Anal. At. Spectrom.*, 2009, **24**, 1364–1372.
14 O. Narygina, M. Mattesini, I. Kantor, S. Pascarelli, X. Wu, G. Aquilanti, C. McCammon and L. Dubrovinsky, *Phys. Rev. B: Condens. Matter Mater. Phys.*, 2009, **79**, 174115.
15 J.-F. Lin, Z. Mao, I. Jarrige, Y. Xiao, P. Chow, T. Okuchi, N. Hiraoka and S. D. Jacobsen, *Am. Mineral.*, 2010, **95**, 1125–1131.
16 G. Schütz, W. Wagner, W. Wilhelm, P. Kienle, R. Zeller, R. Frahm and G. Materlik, *Phys. Rev. Lett.*, 1987, **58**, 737–740.
17 M. M. Schwickert, G. Y. Guo, M. A. Tomaz, W. L. O'Brien and G. R. Harp, *Phys. Rev. B: Condens. Matter Mater. Phys.*, 1998, **58**, R4289.
18 S. Bonhommeau, N. Pontius, S. Cobo, L. Salmon, F. M. F. de Groot, G. Molnar, A. Bousseksou, H. A. Durr and W. Eberhardt, *Phys. Chem. Chem. Phys.*, 2008, **10**, 5882–5889.
19 F. M. F. de Groot, P. Glatzel, U. Bergmann, P. A. van Aken, R. A. Barrea, S. Klemme, M. Hävecker, A. Knop-Gericke, W. M. Heijboer and B. M. Weckhuysen, *J. Phys. Chem. B*, 2005, **109**, 20751–20762.

20 C. Piquer, M. A. Laguna-Marco, A. G. Roca, R. Boada, C. Guglieri and J. Chaboy, *J. Phys. Chem. C*, 2014, **118**, 1332–1346.

21 P. A. van Aken, B. Liebscher and V. J. Styrsa, *Phys. Chem. Miner.*, 1998, **25**, 323–327.

22 P. A. van Aken and B. Liebscher, *Phys. Chem. Miner.*, 2002, **29**, 188–200.

23 C. C. Calvert, A. Brown and R. Brydson, *J. Electron Spectrosc. Relat. Phenom.*, 2005, **143**, 173–187.

24 D. J. Frost, F. Langenhorst and P. A. van Aken, *Phys. Chem. Miner.*, 2001, **28**, 455–470.

25 J. P. Crocombette, M. Pollak, F. Jollet, N. Thromat and M. Gautier-Soyer, *Phys. Rev. B: Condens. Matter Mater. Phys.*, 1995, **52**, 3143–3150.

26 R. K. Hocking, E. C. Wasinger, F. M. F. de Groot, K. O. Hodgson, B. Hedman and E. I. Solomon, *J. Am. Chem. Soc.*, 2006, **128**, 10442–10451.

27 S. Miao, M. Kocher, P. Rez, B. Fultz, R. Yazami and C. C. Ahn, *J. Phys. Chem. A*, 2007, **111**, 4242–4247.

28 T. Kroll, S. Bonhommeau, T. Kachel, H. A. Dürr, J. Werner, G. Behr, A. Koitzsch, R. Hübel, S. Leger, R. Schönfelder, A. K. Ariffin, R. Manzke, F. M. F. de Groot, J. Fink, H. Eschrig, B. Büchner and M. Knupfer, *Phys. Rev. B: Condens. Matter Mater. Phys.*, 2008, **78**, 220502.

29 B. Gilbert, J. E. Katz, J. D. Denlinger, Y. Yin, R. Falcone and G. A. Waychunas, *J. Phys. Chem. C*, 2010, **114**, 21994–22001.

30 H. Wang, G. Peng, L. M. Miller, E. M. Scheuring, S. J. George, M. R. Chance and S. P. Cramer, *J. Am. Chem. Soc.*, 1997, **119**, 4921–4928.

31 N. Bergmann, S. Bonhommeau, K. M. Lange, S. M. Greil, S. Eisebitt, F. M. F. de Groot, M. Chergui and E. F. Aziz, *Phys. Chem. Chem. Phys.*, 2010, **12**, 4827–4832.

32 W. M. Heijboer, A. A. Battiston, A. Knop-Gericke, M. Hävecker, R. Mayer, H. Bluhm, R. Schlögl, B. M. Weckhuysen, D. C. Koningsberger and F. M. F. de Groot, *J. Phys. Chem. B*, 2003, **107**, 13069–13075.

33 W. M. Heijboer, A. A. Battiston, A. Knop-Gericke, M. Havecker, H. Bluhm, B. M. Weckhuysen, D. C. Koningsberger and F. M. F. de Groot, *Phys. Chem. Chem. Phys.*, 2003, **5**, 4484–4491.

34 W. M. Heijboer, P. Glatzel, K. R. Sawant, R. F. Lobo, U. Bergmann, R. A. Barrea, D. C. Koningsberger, B. M. Weckhuysen and F. M. F. de Groot, *J. Phys. Chem. B*, 2004, **108**, 10002–10011.

35 W. Heijboer, D. Koningsberger, B. Weckhuysen and F. M. F. de Groot, *Catal. Today*, 2005, **110**, 228–238.

36 J. P. Wang, N. Ji, X. Liu, Y. Xu, C. Sanchez-Hanke, Y. Wu, F. M. F. de Groot, L. F. Allard and E. Lara-Curzio, *IEEE Trans. Magn.*, 2012, **48**, 1710–1717.

37 J.-F. Lin, H. Fukui, D. Prendergast, T. Okuchi, Y. Q. Cai, N. Hiraoka, C.-S. Yoo, A. Trave, P. Eng, M. Y. Hu and P. Chow, *Phys. Rev. B: Condens. Matter Mater. Phys.*, 2007, **75**, 012201.

38 S. K. Lee, P. J. Eng and H.-k. Mao, *Rev. Mineral. Geochem.*, 2014, **78**, 139–174.

39 S. K. Lee, J.-F. Lin, Y. Q. Cai, N. Hiraoka, P. J. Eng, T. Okuchi, H.-k. Mao, Y. Meng, M. Y. Hu, P. Chow, J. Shu, B. Li, H. Fukui, B. H. Lee, H. N. Kim and C.-S. Yoo, *Proc. Natl. Acad. Sci. U. S. A.*, 2008, **105**, 7925–7929.

40 C. J. Sahle, C. Sternemann, C. Schmidt, S. Lehtola, S. Jahn, L. Simonelli, S. Huotari, M. Hakala, T. Pylkkänen, A. Nyrow, K. Mende, M. Tolan, K. Hämäläinen and M. Wilke, *Proc. Natl. Acad. Sci. U. S. A.*, 2013, **110**, 6301–6306.

41 C. Sternemann, C. J. Sahle, K. Mende, C. Schmidt, A. Nyrow, L. Simonelli, M. Moretti Sala, M. Tolan and M. Wilke, *J. Phys.: Conf. Ser.*, 2013, **425**, 202011.

42 J. S. Tse, L. Yang, S. J. Zhang, C. Q. Jin, C. J. Sahle, C. Sternemann, A. Nyrow, V. Giordano, J. Z. Jiang, S. Yamanaka, S. Desgreniers and C. A. Tulk, *Phys. Rev. B: Condens. Matter Mater. Phys.*, 2011, **84**, 184105.

43 J. S. Tse, M. Hanfland, R. Flacau, S. Desgreniers, Z. Li, K. Mende, K. Gilmore, A. Nyrow, M. Moretti Sala and C. Sternemann, *J. Phys. Chem. C*, 2014, **118**, 1161–1166.

44 A. Nyrow, J. S. Tse, N. Hiraoka, S. Desgreniers, T. Büning, K. Mende, M. Tolan, M. Wilke and C. Sternemann, *Appl. Phys. Lett.*, 2014, **104**, 262408.

45 A. Nyrow, C. Sternemann, M. Wilke, R. Gordon, K. Mende, H. Yavaş, L. Simonelli, N. Hiraoka, C. Sahle, S. Huotari, G. Andreozzi, A. Woodland, M. Tolan and J. S. Tse, *Contrib. Mineral. Petrol.*, 2014, **167**, 1012.

46 N. Hiraoka, M. Takahashi, W. B. Wu, C. H. Lai, K. D. Tsuei and D. L. Huang, *Phys. Rev. B: Condens. Matter Mater. Phys.*, 2015, **91**, 241112(R).

47 U. Bergmann, P. Glatzel and S. P. Cramer, *Microchem. J.*, 2002, **71**, 221–230.

48 W. Schülke, *Electron Dynamics by Inelastic X-Ray Scattering*, Oxford Univ. Press, 2007.

49 K. Hämäläinen and S. Manninen, *J. Phys.: Condens. Matter*, 2001, **13**, 7539.

50 M. Krisch and F. Sette, *Surf. Rev. Lett.*, 2002, **09**, 969–976.

51 C. Sternemann, H. Sternemann, S. Huotari, F. Lehmkühler, M. Tolan and J. S. Tse, *J. Anal. At. Spectrom.*, 2008, **23**, 807–813.

52 R. A. Gordon, G. T. Seidler, T. T. Fister, M. W. Haverkort, G. A. Sawatzky, A. Tanaka and T. K. Sham, *EPL*, 2008, **81**, 26004.

53 M. W. Haverkort, A. Tanaka, L. H. Tjeng and G. A. Sawatzky, *Phys. Rev. Lett.*, 2007, **99**, 257401.

54 T. T. Fister, G. T. Seidler, C. Hamner, J. O. Cross, J. A. Soininen and J. J. Rehr, *Phys. Rev. B: Condens. Matter Mater. Phys.*, 2006, **74**, 214117.

55 C. Krywka, C. Sternemann, M. Paulus, N. Javid, R. Winter, A. Al-Sawalmih, S. Yi, D. Raabe and M. Tolan, *J. Synchrotron Radiat.*, 2007, **14**, 391.

56 H. Sternemann, C. Sternemann, G. T. Seidler, T. T. Fister, A. Sakko and M. Tolan, *J. Synchrotron Radiat.*, 2008, **15**, 162–169.

57 C. J. Sahle, A. Mirone, J. Niskanen, J. Inkinen, M. Krisch and S. Huotari, *J. Synchrotron Radiat.*, 2015, **22**, 400–409.

58 C. Colliex, T. Manoubi and C. Ortiz, *Phys. Rev. B: Condens. Matter Mater. Phys.*, 1991, **44**, 11402–11411.

59 J. H. Paterson and O. L. Krivanek, *Ultramicroscopy*, 1990, **32**, 319–325.

This journal is © The Royal Society of Chemistry 2016

J. Anal. At. Spectrom., 2016, **31**, 815–820 | 819

60 R. A. Gordon, M. W. Haverkort, S. Sen Gupta and G. A. Sawatzky, *J. Phys.: Conf. Ser.*, 2009, **190**, 012047.

61 L. A. J. Garvie and P. R. Buseck, *Nature*, 1998, **396**, 667–670.

62 T. Manoubi, M. Tencé and C. Colliex, *Ultramicroscopy*, 1989, **28**, 49–55.

63 H. K. Mao, J. Xu and P. M. Bell, *J. Geophys. Res.*, 1986, **91**, 4673–4676.

64 V. Cerantola, C. McCammon, I. Kupenko, I. Kantor, C. Marini, M. Wilke, L. Ismailova, N. Solopova, A. Chumakov, S. Pascarelli and L. Dubrovinsky, *Am. Mineral.*, 2015, **100**, 2670.